batteries

Article

Thermal Propagation Test Bench for the Study of the Paschen Curve and Lightning Arcs of Venting Gas

Björn Mulder [1], Kai Peter Birke [1,*], Björn Obry [2], Stefan Wigger [2], Ruslan Kozakov [3], Pavel Smirnov [3] and Jochen Schein [3]

[1] Institute for Photovoltaics, University of Stuttgart, Pfaffenwaldring 47, 70569 Stuttgart, Germany
[2] Mercedes-Benz Group AG, Mercedesstraße 120, 70372 Stuttgart, Germany
[3] Institute for Plasma Technology and Basics of Electrical Engineering, Bundeswehr University Munich, Werner-Heisenberg-Weg 39, 85579 Neubiberg, Germany
* Correspondence: peter.birke@ipv.uni-stuttgart.de

Abstract: Thermal propagation events are characterized by fire and thick black smoke, leading to propagation methods with a focus on preventing heat transfer and optimizing gas flow. Yet little attention is being paid to the electric conductivity of the gas, leading to possibly unexpected battery casing openings due to lightning arcs as well as potentially providing the minimum ignition energy. This gas composition (omitting particles) was used at different temperatures and pressures in a lightning arc test bench, leading to the Paschen curve. Using a mini-module cell setup, filtered venting gas was flowed through another lightning arc test bench, allowing for in situ measurements.

Keywords: thermal runaway; thermal propagation; lightning arcs; Paschen's law; test bench

check for updates

Citation: Mulder, B.; Birke, K.P.; Obry, B.; Wigger, S.; Kozakov, R.; Smirnov, P.; Schein, J. Thermal Propagation Test Bench for the Study of the Paschen Curve and Lightning Arcs of Venting Gas. *Batteries* **2024**, *10*, 397. https://doi.org/10.3390/batteries10110397

Academic Editors: Prodip K. Das and Pascal Venet

Received: 12 September 2024
Revised: 16 October 2024
Accepted: 22 October 2024
Published: 8 November 2024

Copyright: © 2024 by the authors. Licensee MDPI, Basel, Switzerland. This article is an open access article distributed under the terms and conditions of the Creative Commons Attribution (CC BY) license (https://creativecommons.org/licenses/by/4.0/).

1. Introduction

With the rise in electric vehicles comes the need for the public to understand and predict possible safety issues compared to well-known internal combustion engine cars. A select number of incidents showing the destructiveness of battery fires have been recorded by Sun et al. [1].

The perceived threat of battery fires, typically due to thermal propagation, has caused governments across the globe to implement legislation in order to reduce the potential overall occurrence of said fires as well as their individual severity, most notably the UN Global Technical Regulation GTR 20 [2]. The current legislation aims to delay propagation to ensure sufficient passenger evacuation time windows. For this, the thermal parameters of the battery such as the cells and parts need to be well tailored.

The venting of the initial cell introduces a new environment into the battery: this venting gas contains flammable components at high temperatures as well as particles of various sizes and compositions. The abrasive nature of these particles in the flow as well as the high temperatures may lead to previously protected components losing their safeguards. As a result, previous air and creepage distances in normal operation may not be sufficient or be rendered useless [3].

To better understand the phenomenon, a single NMC 622 lithium ion pouch cell was placed in an autoclave with atmospheric gas composition; thermal runaway was triggered and the venting gas composition was evaluated. The breakdown voltage of this gas at different temperatures was then analyzed and compared to the Paschen curve of air. A breakdown voltage detector for the use of venting gas from cells undergoing thermal runaway was introduced, and the gas was filtered to remove particles. Experiments by Li et al. [4] used a setup with particles in the venting gas.

2. Materials and Methods

In earlier works, single battery cells were placed in autoclaves, triggered into thermal runaway and the released venting gas amount and composition was evaluated, namely in the work of Koch et al. [5]. The most commonly found components are CO_2, CO and H_2 ranging typically around 10–40 %, followed by C_2H_4 and CH_4 at 5–10% and a multitude of trace gases, most notably C_2H_6 and C_3H_6 at around 1% or below.

For the following experiments, a pouch cell with a $LiNi_6Mn_2Co_2O_2$ (NMC 622)-cathode was used. The relevant cell is seen in Figure 1 and its characteristics before testing are as follows:

- $\rho_{vol} \approx 500\,\mathrm{Wh}\ell^{-1}$
- $E_{capacity} \approx 60\,\mathrm{Ah}$

Figure 1. Pouch cell under investigation with cell tabs on the side.

2.1. Venting Gas Mixture from Autoclave Setup

An autoclave has a reinforced container at its center, allowing to observe chemical reactions at different temperatures and pressures with hermetic sealing and pressure resistance of the reaction chamber. The used autoclave has a volume of 80 ℓ and is initially filled with air; the cell is placed inside the autoclave and brought into thermal runaway (TR) using a heater. Once the TR has stopped and the autoclave has cooled to ambient temperatures, a gas sample is taken. The gas analysis is then performed by a gas chromatograph.
The following results for the venting gas were yielded from averaging multiple experiments with cells tested with a SoC (State of Charge) of 100%:

$c_{N_2} = 35.4$ vol%, $c_{CO_2} = 24.0$ vol%, $c_{CO} = 21.0$ vol%, $c_{H_2} = 13.0$ vol%, $c_{C_2H_4} = 3.6$ vol% and $c_{CH_4} = 3$ vol%.

The artificial venting gas used in the experiments that follow was manufactured accordingly, including nitrogen. During thermal propagation, the gas composition within a battery changes rapidly, as the initial nitrogen gets pushed out due to more cells undergoing thermal runaway, and the initial oxygen is quickly reacted. Lightning arc events can already occur during the venting of the initial cell. Thus, the artificial venting gas should contain nitrogen for a better understanding of the breakdown voltage in venting gas. This paper focuses on the gas component; particles were omitted from the artificial venting gas as a first step in analyzing the arcing phenomenon.

2.2. Paschen's Law

Paschen's law describes an equation of the necessary voltage between two electrodes in a gas for a discharge or electric arc to occur ([6–9]). The influencing parameters include the specific type of gas, pressure, temperature, and distance/gap between electrodes, as well as the shape of the electrodes. Graphs typically show the breakdown voltage as a function $f(d \cdot p)$ of distance d and pressure p with the abscissa typically in a log scale. The curves for various gases as well as air are shown in Figure 2, given by Celani et al. [10]. The parameter of Paschen's law for mixtures of gases cannot be calculated from its individual gas components, so testing is unavoidable. The used gas composition was gathered by the autoclave testing described in Section 2.1.

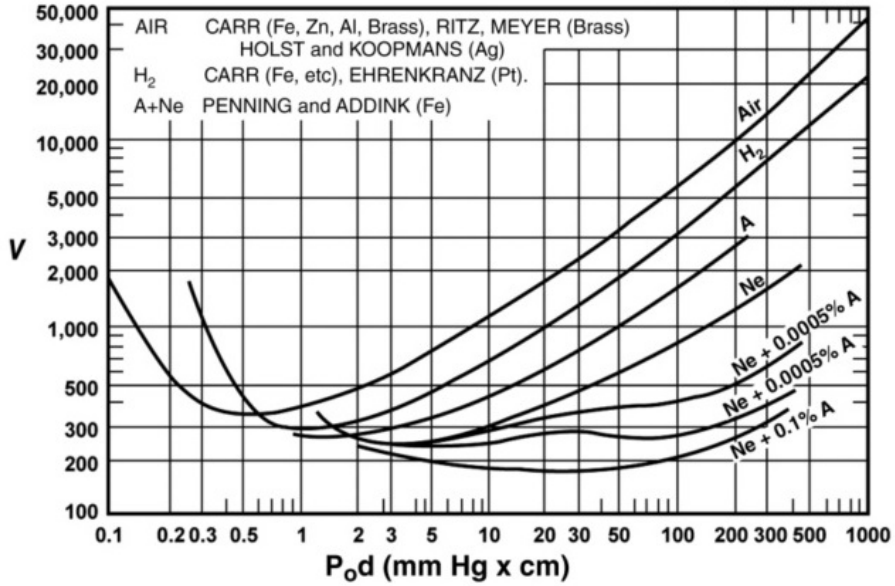

Figure 2. Overview of different Paschen curves, most notably of air; see Lehr and Ron [11]. 1 mm Hg · cm ≈ 13.3 mbar · mm.

According to Lehr and Ron [11], the Paschen curve can be described using the equation

$$V_b = \frac{B \cdot (pd)}{ln(pd \cdot A) - ln(ln(1 + \gamma^{-1}))} \tag{1}$$

with V_b being the breakdown voltage, p the pressure, d the distance between the electrodes, A and B the gas-specific constants, and γ the third Townsend coefficient. For large values of (pd), coefficient γ is negligible, and Equation (2) simplifies to

$$\lim_{(pd)\to\infty} V_b \approx \frac{B \cdot (pd)}{ln(pd \cdot A)} \tag{2}$$

Two points $(pd)_1$ and $(pd)_2$ can be selected with their respective arcing voltages $V_b((pd)_1)$ and $V_b((pd)_2)$, leading to value B being expressed as

$$B \approx \frac{V_b((pd)_1) \cdot ln((pd)_1 \cdot A)}{(pd)_1}; \qquad B \approx \frac{V_b((pd)_2) \cdot ln((pd)_2 \cdot A)}{(pd)_2} \tag{3}$$

These two Equations (3) can now be equated to

$$\frac{V_b((pd)_1)}{(pd)_1} \cdot ln((pd)_1 \cdot A) \approx \frac{V_b((pd)_2)}{(pd)_2} \cdot ln((pd)_2 \cdot A) \tag{4}$$

Rearranging and solving for A allows for the approximate calculations of A and B as

$$A \approx e^{\left[\frac{\frac{V_b((pd)_1)}{(pd)_1} \cdot ln((pd)_1) - \frac{V_b((pd)_2)}{(pd)_2} \cdot ln((pd)_2)}{\left(\frac{V_b((pd)_2)}{(pd)_2} - \frac{V_b((pd)_1)}{(pd)_1}\right)}\right]}; \text{ for large } (pd) \tag{5}$$

$$B \approx \frac{V_b(pd) \cdot ln((pd) \cdot A)}{(pd)}; \text{ for large } (pd) \tag{6}$$

2.3. Breakdown Voltage Detector

The breakdown voltage detector is designed for pressures of p = 10 mbar–1500 mbar and temperatures up to $T_{max} \approx 1000$ °C. The separation between the electrodes is adjusted by a stepper motor to allow distance increments of $d_{step} = 3.125 \cdot 10^{-3}$ mm.

A schematic cross section of the used breakdown voltage detector is shown in Figure 3: A pair of electrodes (1) is placed in a glass cylinder containing a gas specimen. Inner isolators (2) and outer isolators (3) keep the gas within while also allowing the manipulator (4) to change the position of the left electrode; the volume between the left and right electrode is called the test gap. The manipulator is connected to a stepper motor to allow direct discrete distances in multiples of $3.125 \cdot 10^{-3}$ mm. Pressure levels are measured using a Pirani gauge (5); gas inlets (6) allow to attach gas cylinders, and a valve connector (7) connects to a vacuum pump.

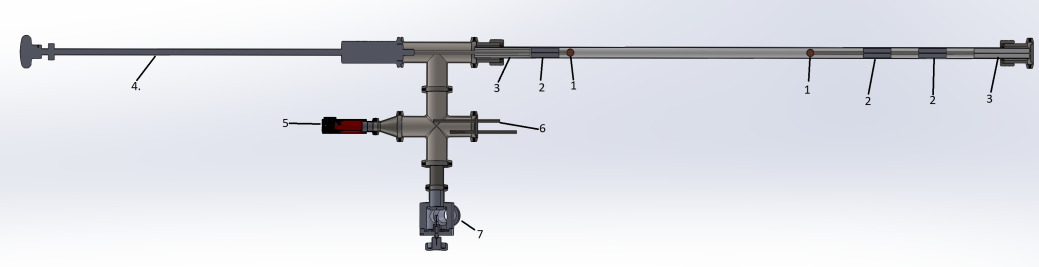

Figure 3. Schematic overview of the breakdown voltage detector. (1) Pair of electrodes, (2) inner isolaters, (3) outer isolators, (4) manipulator, (5) Pirani gauge, (6) gas inlet, and (7) valve connector.

In previous work (see Mulder et al. [12]), it was shown that a module of 12 pouch cells with a SoC of 100% can deliver peak temperatures of around 900 °C. To recreate these temperatures, a small brick box with heating elements acting as a brick oven is used. The test gap of the breakdown voltage detector can be placed within the heated volume, which can deliver temperatures up to the required 900 °C as seen in Figure 4.

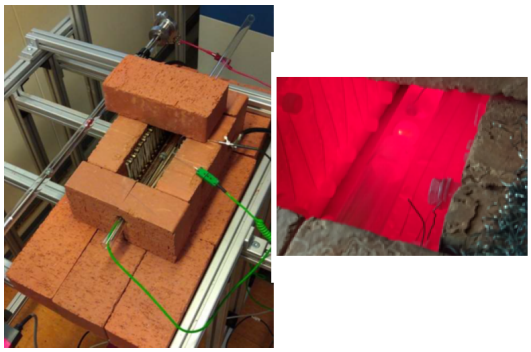

Figure 4. For tests at higher temperatures, the test gap of the breakdown voltage detector can be placed inside a brick oven. (**Left**) Test bench at room temperatures, (**Right**) test bench with activated heating elements.

Before experiment data can be collected, the vacuum pump attached to the outlet valve (7) evacuates the main glass cylinder. Then, the cylinder can be filled using the gas inlets (6) from attached gas bottles; for higher gas purity, the process of gas evacuation and refilling can be repeated. The inner (2) and outer (3) isolators prevent undesired gas from bleeding into the test gap. Initially, a set of glass cylinder and electrodes (set A) was used, which was later replaced with a new glass cylinder, and the electrodes were equipped with additional alignment (set B); both sets can be seen in Figure 5. An overview of the experiments carried out using venting gas with different temperature/pressure points can be found in Table 1.

Figure 5. (**Left**) Cylinder and electrode set A, (**Right**) cylinder and electrode set B, with additional supporting alignment. The electrodes are manufactured from copper.

Table 1. Overview of experiments with venting gas: temperature T, pressure p and glass cylinder/electrode set (A or B) combinations.

Gas	$p = 1250$ **mbar**	$p = 1500$ **mbar**
Cylinder A		
200 °C	X	X
500 °C	X	X
900 °C	X	X
Cylinder B		
200 °C	X	X
500 °C	X	X
900 °C	X	X

2.4. Venting Gas Breakdown Voltage Detector

The test facility, seen in Figure 6, can be split into three functional groups: the mini-module test bench (red box), the exhaust system with measurement equipment (blue box), and the surrounding environment. All components were selected and designed with robustness in mind to ensure a high level of safety during testing as well as its reusability. A more detailed description of the capabilities and experiment setup can be found in the previous publication by Mulder et al. [12]. A schematic overview of the entire test setup can be seen in Figure 7.

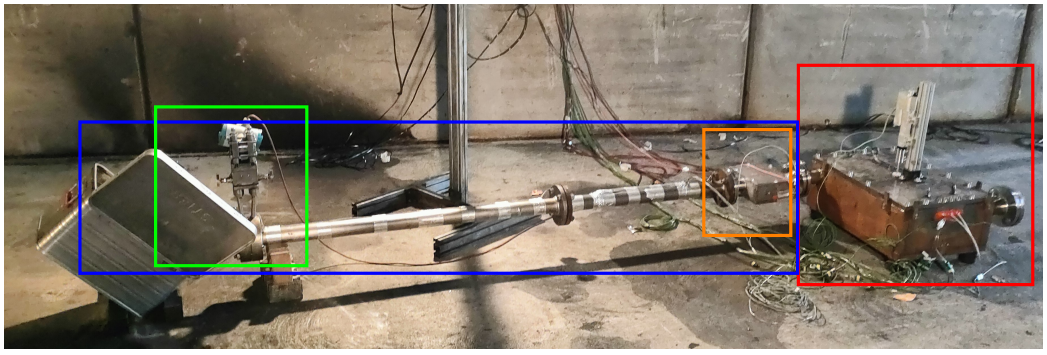

Figure 6. Overview of the test facility: the mini-module test bench (in red box) is connected via flanges to the exhaust system (blue box), which allows the generated venting gas to vent into the surrounding environment—a metal box is placed at the end to allow the capture of particles. Within the exhaust system, the lightning arc box (orange box) is placed, as well as a mass flow meter (green box).

The opened mini-module test bench can be seen in Figure 8, where a custom cell stack of mid-of-life 6 2p3s-connected pouch cells are placed. An edge cell of the pack is triggered, ensuring that cells propagate one after another instead of up to two cells simultaneously. The used trigger method is nail penetration with a wedge-shaped nail parallel to the electrode layers. Other trigger methods can be implemented yet were not chosen for the lightning arc study.

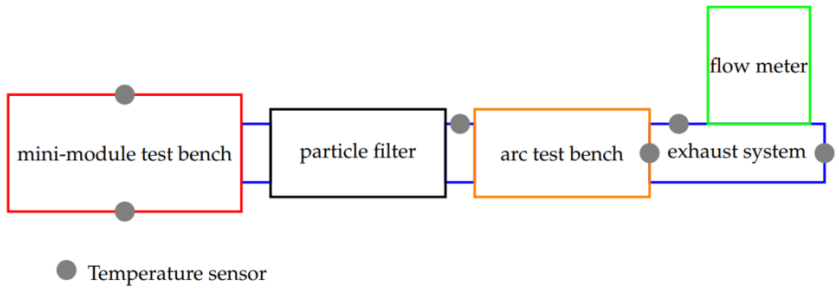

Figure 7. Schematic overview of the test facility: cells can be triggered in the mini-module test bench, and exhaust travels through the particle filter and the arc test bench out of the exhaust pipe into the surrounding environment. Temperature sensors placed outside of the mini-module test bench are shown.

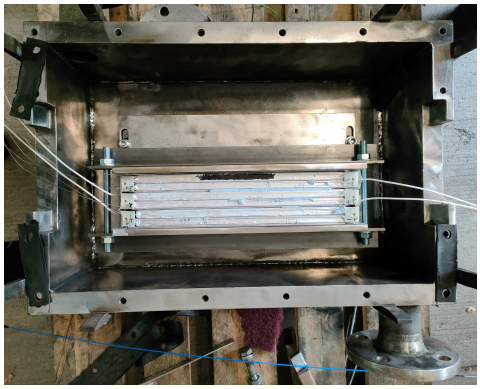

Figure 8. View into the opened test bench: A mini-module of 2p3s-connected pouch cells is placed inside the test mount. The nail gun will trigger the topmost cell marked with a black stripe.

In the exhaust line (see Figure 6), the lightning arc box can be installed using the flange system. The opened box can be seen in Figure 9: two electrodes with a diameter of 25 mm are connected to the power supply and voltage measurement equipment. Using feeler gauges, the appropriate distance can be set, as well as ensuring that the flat surfaces are parallel to each other. The studied gas can flow in a pipe made of two PEEK pieces. Before testing, the other half of the pipe piece is placed and sealed. Loctite SI 5300 is used as a sealant around the electrode rod as well as in between the pipe pieces and the lid of the lightning arc box.

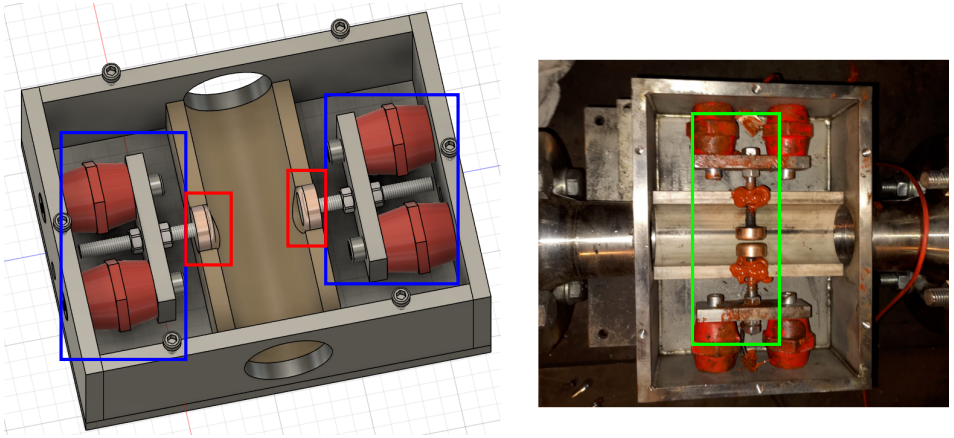

Figure 9. (**Left**) Schematic view of the lightning arc box. (**Right**) View of the lightning arc box before closing. Circular electrodes (red box) are attached via electrode rods (blue box) to the power supply. The bottom half of the PEEK pipe (green box) is already installed.

2.4.1. Testing Procedure Setup

The cell block is charged to 100% SoC and placed in the test bench. The cell mount is adjusted to ensure that the nail gun (later attached to the lid) will only trigger one cell. Before the lid is placed on the test bench, Loctite SI 5300 is applied to create a gastight seal. Screws and a clamping system secures the lid in place. The test bench has two flanges placed diagonally from each other: to one flange of the test bench, an end flange is connected, and to the other flange, the exhaust system is connected. It consists of a pipe system of the lightning arc box and the mass flow meter; a particle filter can be implemented in the exhaust pipe, placed before the arc box. To the lightning arc box, a power supply is wired. Once the mechanical setup is complete, the voltage to the electrodes is initially set at 50 V; after every vented cell, it is to be increased by 50 V. The cell pack is triggered by a nail gun, which is attached to the top side of the lid. Two cameras are set up. The first focuses on the test bench with the attached nail gun; the second camera records the venting gas leaving the end of the exhaust system.

2.4.2. Sensors and Placement

The following measurement data are collected: (1) initial time of nail penetration, (2) temperature within the cell block, test bench, exhaust system and environment, (3) voltage of the cell block and lightning arc box, and (4) massflow in exhaust system.

1. Initial time of nail penetration
   It is recorded when and for how long the nail gun motor is activated—once the nail is fully inserted into the cell, the motor stops.
2. Temperature sensors
   Type K sensors are used; a schematic overview can be seen in Figure 10. Four sensors are placed within the cell mount/cell stack and are numbered, using aluminum plates with sensor cutout to avoid indentation into the cells. Two sensors are placed on the connection between cell mount and test bench, two in the test bench (top and bottom), four along the exhaust system, and one recording the surrounding environment.
3. Voltage metering
   Voltage is measured in the cell pack—every logical cell (2p) as well as the overall stack are measured. The electrodes within the lightning arc box are supplied with the appropriate voltage, yet to record the lightning arc, a sufficiently fast voltmeter needs to be used. To detect the presence of lightning arcs, 100 Hz is found to be sufficient.
4. Massflow
   A SITRANS P320 digital pressure transmitter allows for gas flow (and thus gas creation) measurement of venting gas during the TP process.

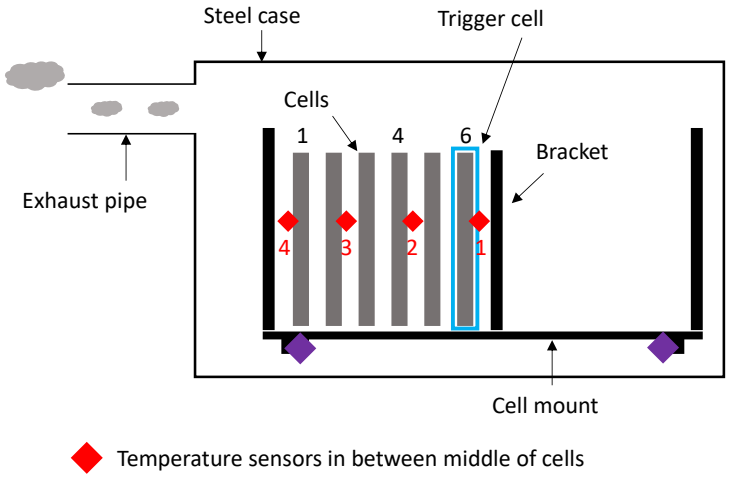

Figure 10. Schematic overview of temperature sensor placement in the test bench: 4 centrally located between cells, respectively between the cells and cell mount, and numbered starting with 1 from the trigger cell towards the exhaust pipe.

3. Results

3.1. Breakdown Voltage Detector Experiments

During one experiment run using the breakdown voltage detector, one combination of gas composition, pressure, and temperature is used (see Table 1). The distance between the electrodes is variable and set by a stepper motor. The procedure of the breakdown curve measurement starts from moving the electrodes together until the short circuit is detected. After that, one electrode is driven away by the stepper motor by one step in 500 ms. The position at which the short circuit disappears is taken as the smallest distance of $3.125 \cdot 10^{-3}$ mm. This procedure makes the accuracy of the electrode separation measurement equal to that of the stepper motor resolution, eliminating the dependence on thermal expansion at different temperatures. For each distance, the voltage is increased until an abrupt drop occurs: a lightning arc with the breakdown voltage is detected and recorded. Then, the stepper motor moves one step further, and the process repeats.

3.1.1. Air

The breakdown voltage detector is filled with air at $T = 100$ °C. In Figure 11, the breakdown voltage for pressures $p = 2.2$ mbar and $p = 5.6$ mbar is recorded. For each pressure, two curves are recorded. It can be seen that the minimum voltage recorded is around 400 V. Lehr and Ron [11] place the lowest breakdown voltage at around 350 V. The range of the breakdown voltage detector presented here therefore has a margin of error of around 10–15 % and is sufficient for the measurement of the breakdown voltage of other gases.

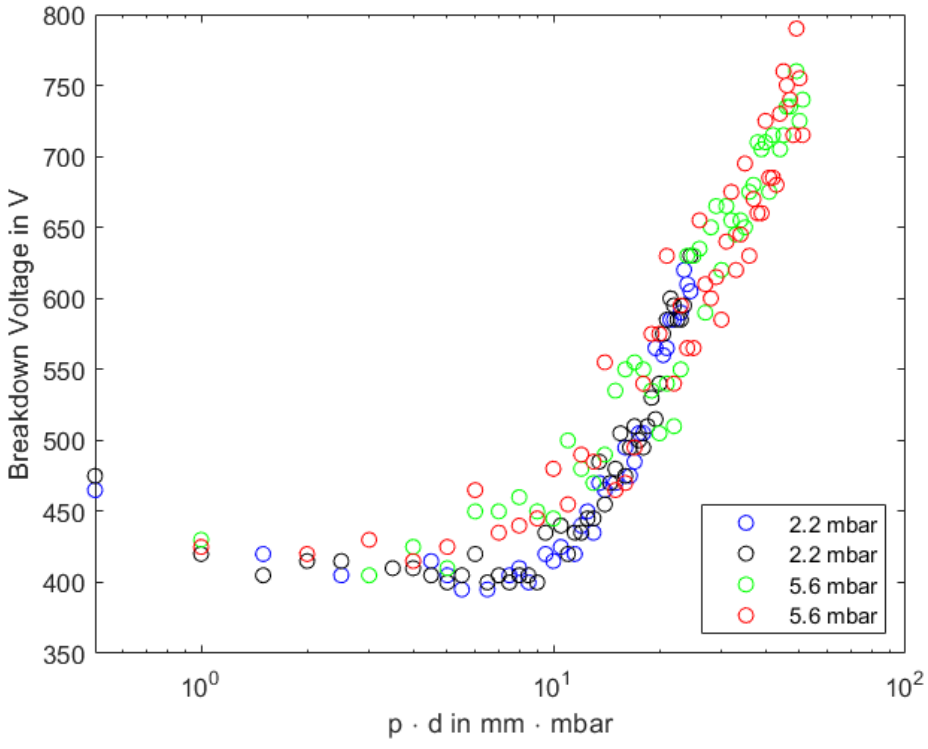

Figure 11. Breakdown voltage detected for Air at $T = 100$ °C for pressures $p = 2.2$ mbar and $p = 5.6$ mbar.

3.1.2. Venting Gas

In Figure 12, the breakdown voltage for the experiments with venting gas (see Table 1) is displayed. It can be seen that higher temperatures result in lower breakdown voltages for higher distances. It needs to be noted that the abscissa is dependent on the pressure and distance ($p \cdot d$) and in log scale. The distances in the experiment are from $d = 3.125 \cdot 10^{-3}$ mm to $d = 1.625 \cdot 10^{-1}$ mm small. The lowest recorded voltage is 330 V, which is lower than

the voltage of 400 V recorded for air at 100 °C at $p = 1$ bar. This would suggest that the venting gas mixture could be more susceptible to lightning arcs than air.

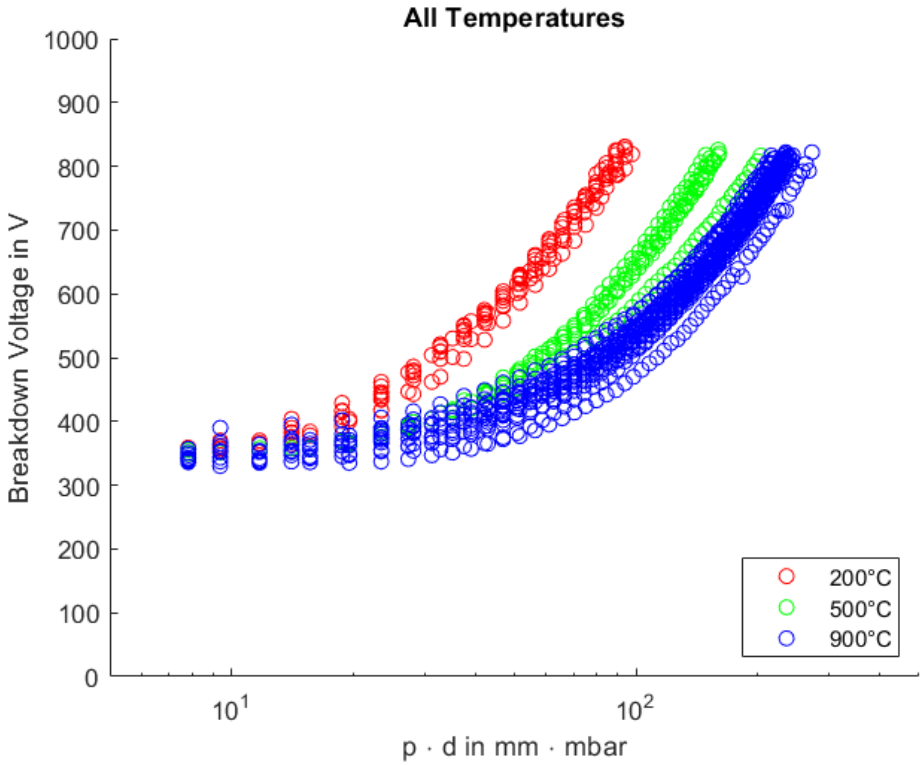

Figure 12. Recorded breakdown voltage for experiments with temperatures $T = 200\,°C$ (Red), 500 °C (Green) and 900 °C (Blue).

In Figure 13, the averaged Paschen curve for venting gas at 200 °C is visualized. The measurement data are plotted in red, while the blue curve is added using the simplified Paschen's law for large $p \cdot d$ according to Equation (2). The lowest recorded breakdown voltage is 350 V at 4.6875 mm · mbar. Compared to 100 °C air at around 400 V, this is a 12.5% decrease. Lehr et al. have analyzed the dependence of the cathode materials in hydrogen while recording the breakdown voltage. It can be clearly seen that the copper electrodes show a minimum breakdown voltage of 295 V, while commercial aluminum shows a minimum voltage of 255 V—copper has a 15.6% higher breakdown voltage compared to commercial aluminum. As the used electrodes for the breakdown voltage detector are made from copper, the noted breakdown voltage for this experiment at 200 °C should be reduced by that percentage, as the materials within a battery are a mixture of multiple metals with casings mainly made from aluminum [13]. This leaves an adjusted voltage of 295.4 V.

In Figure 14, the same curve for 900 °C is shown. The measurement data are again plotted in red, while the blue curve is added using the simplified Paschen's law for large $p \cdot d$ according to Equation (2). The lowest recorded breakdown voltage is 330 V at 9.375 mm · mbar. To adjust the breakdown voltage according to Figure 15 by 15.6%, an adjusted breakdown voltage of 278.52 V can be noted.

According to DIN EN 60664-1 [14], a suitable distance to prevent breakdown voltages in 400 V environments is 0.8 mm. Assuming no excess pressure during venting gas creation, thus setting the pressure to $p = 1000$ mbar, a 0.8 mm distance would require a voltage of ≈1850 V for a lightning arc to occur. The artificial gas is at pressure levels and near thermal propagation temperatures, yet the necessary voltages for a lightning arc in said artificial gas cannot be achieved by a typical traction battery, even if considering 800 V vehicles. Figure 14 shows low voltages in the 300 V–800 V range, yet these are only recorded at low $p \cdot d \leq 300\,\text{mm} \cdot \text{mbar}$. As the real venting gas also has a variety of particles, and lightning

arcs have been observed during TP (Sun et al. [1]), the Paschen's curve analysis indicates that particles need to be part of the observation.

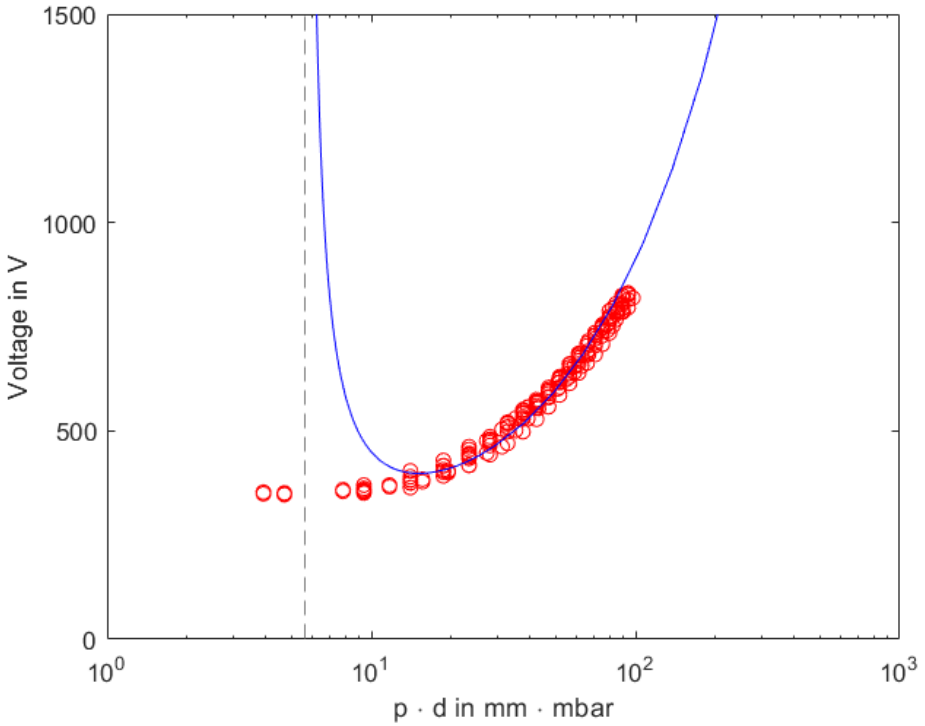

Figure 13. Paschen curve of venting gas at $T = 200\,^{\circ}\mathrm{C}$. The experimental data are shown in red, while the blue curve is generated using the simplified Paschen's law for large $p \cdot d$ (see Equation (2)).

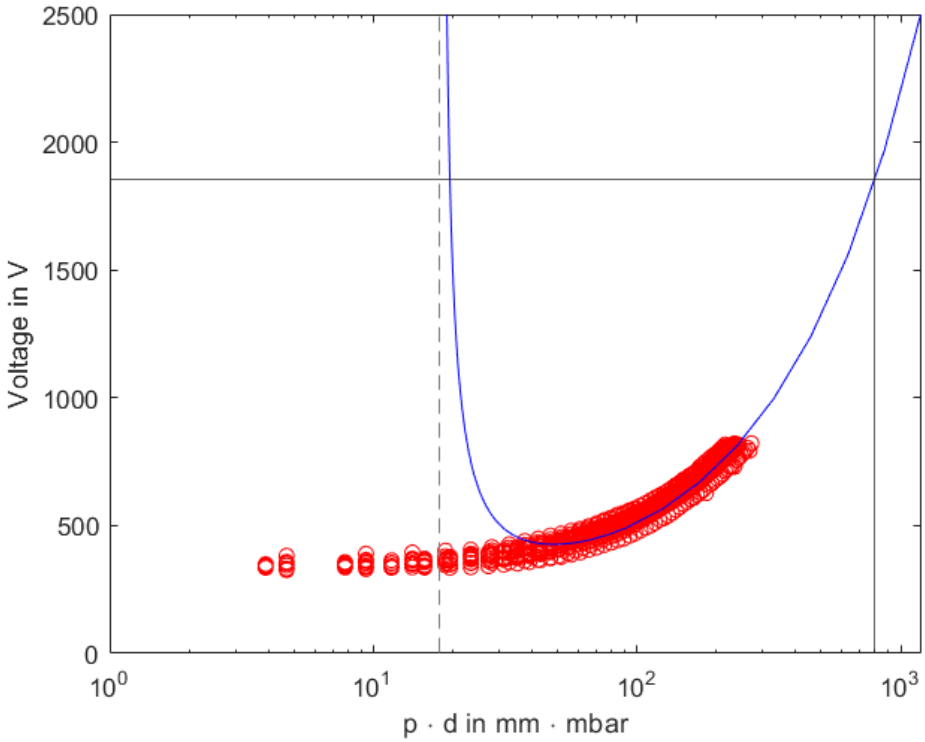

Figure 14. Paschen curve of venting gas at $T = 900\,^{\circ}\mathrm{C}$. The experimental data are shown in red, while the blue curve is generated using the simplified Paschen's law for large $p \cdot d$ (see Equation (2)). For a typical breakdown voltage of 800 V, a distance of 0.8 mm is required for air and creepage distances from the regulatory body [14]—yet the graph shows a required voltage of 1850 V for an arc.

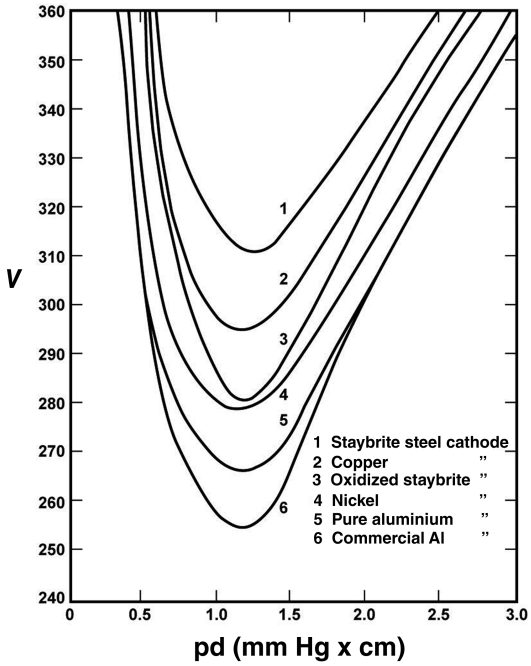

Figure 15. Influence of the cathode materials using Hydrogen when recording the breakdown voltage. Taken from Lehr et al. [11].

3.2. Thermal Propagation Testing

The results of the breakdown voltage detector in Section 3.1 lead to the conclusion that the gaseous part of the venting gas might not be responsible for the lightning arc phenomenon. To verify this, a cell module is triggered to undergo thermal propagation in order to generate real venting gas. In the exhaust pipe, a particle filter is installed, allowing for the study of the venting gas without particles.

A pouch cell mini-module is triggered and undergoes thermal runaway as seen in Figure 16. The electrodes are set to a distance of 2.5 mm $\pm$ 0.5 mm. A distance of 4 mm previously saw arcing, yet experiments using 2 mm are discussed in detail by Li et al. [4]. Before triggering the first cell, the voltage of the lightning arc box was raised to 400 V—during the entire experiment, the voltage did not drop—showing that no lightning arc occurred. Experiments short-circuiting the electrodes showed rapid voltage drops and returns to the preset voltage once the short was removed. The temperature sensor 1 next to the triggered cell showed an immediate rise in the temperature. Sensors 2 and 3 later showed the propagation through the module with temperature peaking between 800 °C and 850 °C, which are near the tested temperatures for the Paschen curves Section 3.1. The numbering of these temperature sensors can be seen in Figure 10.

The experiment showed an absence of drops in the applied voltage to the electrode set in the lightning arc box. The distance of the electrodes used is more than sufficient according to DIN EN 60664-1 [14] for clear clean air. Combining the results from Section 3.1 regarding the Paschen curve, where arcing with 400 V requires distances well below 0.8mm, and the results from the lightning arc box testing, it hints at the conclusion that the gaseous part of the venting gas does not contribute to the lightning arcs observed in traction battery testing. Testing regarding venting gas including particles therefore needs to be carried out and is planned for future publication ([15–21]).

Experiments by Li et al. [4] clearly showed significant arcing at a distance of 2 mm using 316 V of DC power. To a lesser degree, it was also shown that a 4 mm distance experienced arcing. The difference between the experiments by Li et al. and the experiment presented here is the absence of particles in the experiment presented here—which aims to show the influence of particle-free venting gas.

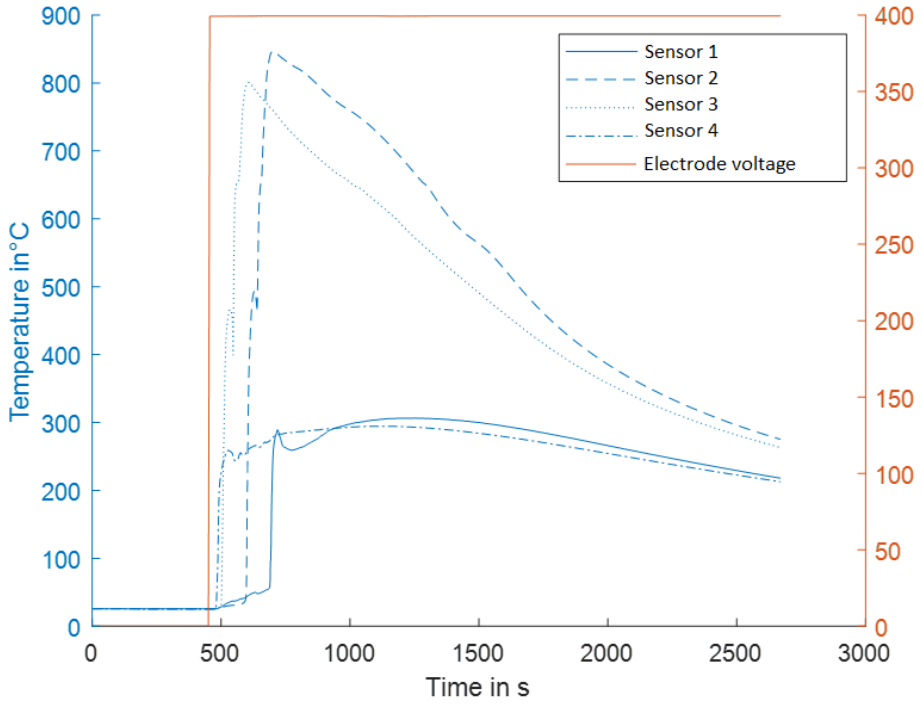

Figure 16. Cell module is triggered and undergoes thermal propagation. The temperature sensors $TB02$ and $TB03$ indicate a reaction, yet the recorded voltage once set to 400 V does not drop. The correlating sensor with its position can be seen in Figure 10.

4. Conclusions

Research regarding thermal propagation is mainly focused on the spread of the event by looking at heat transfer and gas flow. However, researching the electric conductivity of the venting gas can lead to the explanation of battery casing openings due to lightning arcs. Using an autoclave, cells underwent thermal runaway, and the resulting venting gas used was analyzed to contain a mixture of mainly N_2, CO_2, CO and H_2 with a low single-digit percentage of hydrocarbons; artificial venting gas was manufactured accordingly. A breakdown voltage detector was designed with two electrodes in a glass cylinder, allowing for the testing of different gases at pressure levels ranging p = 10–1500 mbar up to gas temperatures of $T \approx 1000$ °C. Paschen curves for $T = 200$ °C and $T = 200$ °C have been determined. For $T = 200$ °C, the lowest recorded breakdown voltage is 350 V at $p \cdot d = 4.6875\,\text{mm} \cdot \text{mbar}$—for $T = 900$ °C, the respective voltage is 330 V at $p \cdot d = 9.375\,\text{mm} \cdot \text{mbar}$.

In order to use real venting gas from a cell pack, a test bench for a pouch cell mini-module with an attached lightning arc box was developed. A particle filter was installed between the test bench and the lightning arc box. The applied voltage to the electrodes of the lightning arc box was set to 400 V, and the distance between the electrodes was set to $d = 2.5\,\text{mm} \pm 0.5$ mm. Using nail penetration, the cell pack was triggered into thermal propagation, and no lightning arcs were detected. This is consistent with the results of the breakdown voltage detector. The literature has shown that a distance of 4 mm with a voltage of 316 V DC in venting gas including particles shows sign of arcing. Both experimental setups confirmed that the required breakdown voltage of venting gas without particles is higher than the typical battery voltage of 400 V. Future experiments should be carried out without the particle filter. The modular setup of the venting gas breakdown voltage detector allows for the easy removal of the particle filter for full venting gas analysis. Additionally, particles will be analyzed for their composition and typical sizes.

Author Contributions: Conceptualization, B.M., B.O. and K.P.B.; methodology, B.M.; software, B.M.; validation, B.M., B.O., P.S. and R.K.; formal analysis, B.M., P.S. and R.K.; investigation, B.M.; resources, B.M. and B.O.; data curation, B.O., P.S. and R.K.; writing—original draft preparation, B.M.; writing—review and editing, B.M.; visualization, B.M.; supervision, B.O., J.S. and K.P.B.; project administration, B.M., B.O. and S.W.; funding acquisition, B.O. and S.W. All authors have read and agreed to the published version of the manuscript.

Funding: The experiments and materials were financed by Mercedes-Benz.

Institutional Review Board Statement: Not applicable.

Informed Consent Statement: Not applicable.

Data Availability Statement: Data are contained within the article.

Acknowledgments: The authors thank Stephan Zimmermann for his expertise on the experimental design of the breakdown voltage detector.

Conflicts of Interest: The authors declare no conflicts of interest.

Abbreviations

The following abbreviations are used in this manuscript:

UN-ECE	United Nations Economic Commission for Europe
GTR	Global Technical Regulations
NMC	Nickel Manganese Cobalt battery chemistry
CO_2	Carbon Dioxide
CO	Carbon Monoxide
H_2	Hydrogen
C_2H_6	Ethane
CH_4	Methane
TR	Thermal Runaway
TP	Thermal Propagation
SoC	State of Charge
D_2	Deuterium
2p3s	Battery cells connected: 2 parallel in a series of 3
PEEK	Polyetheretherketone
DIN EN #	German edition of European standards

References

1. Sun, P.; Bisschop, R.; Niu, H.; Huang, X. A Review of Battery Fires in Electric Vehicles. *Fire Technol.* **2020**, *56*, 1361–1410. [CrossRef]
2. Global Technical Regulation on the Electric Vehicle Safety (EVS). Available online: https://unece.org/fileadmin/DAM/trans/main/wp29/wp29wgs/wp29gen/wp29registry/ECE-TRANS-180a20e.pdf/ (accessed on 1 July 2023).
3. Wang, Q.; Ping, P.; Zhao, X.; Chu, G.; Sun, J.; Chen, C. Thermal runaway caused re and explosion of lithium ion battery. *J. Power Sources* **2012**, *208*, 210–224. [CrossRef]
4. Li, Z.; Liu, D.; Li, H.; Dong, W.; Zhang, H.; Tian, Y.; Liu, L. Experimental Study on Arcing in Thermal Propagation of Lithium-Ion Battery Systems. Available online: https://ouci.dntb.gov.ua/en/works/4gZAvYr7/ (accessed on 27 October 2024).
5. Koch, S.; Fill, A.; Kai Peter Birke, L. Comprehensive gas analysis on large scale automotive lithium-ion cells in thermal runaway. *J. Power Sources* **2018**, *398*, 106–112. [CrossRef]
6. Spektrum der Wissenschaft Verlagsgesellschaft mbH, Hrsg. Gasentladung. 4 December 2004. Available online: https://www.spektrum.de/lexikon/physik/gasentladung/5555 (accessed on 27 October 2024).
7. Kuechler, A. *Hochspannungstechnik: Grundlagen-Technologie-Anwendungen*; Springer: Heidelberg, Germany, 2009; ISBN 978-3- 540-78412-8.
8. Roth, A. *Hochspannungstechnik*, 4th ed.; Springer: Vienna, Austria, 1959; ISBN 978-3-7091-3904-2.
9. Hopf, A. Elektrische Festigkeit von SF6 und Alternativen Isoliergasen (Luft, CO_2, N_2, O_2 und C3F7CN-Gemisch) bis 2,6 MPa. Ph.D. Dissertation, Technische Universität Ilmenau, Ilmenau, Germany, 2020. [CrossRef]
10. Celani, F.; Lorenzetti, C.; Vassallo, G.; Purchi, E.; Fiorilla, S.; Cupellini, S.; Nakamura, M.; Cerreoni, P.; Burri1, R.; Boccanera, P.; et al. Clear and simple evidence of correlations among Open Voltage values and AHE in Constantan wires, DC operations under H2 gas, after long time conditioning at 70 and 100 W of input power. In Proceedings of the IWAHLM14, Assisi, Italy, 29 August–1 September 2021. [CrossRef]
11. Lehr, J.; Ron, P. *Foundations of Pulsed Power Technology*, 1st ed.; Wiley: Hoboken, NJ, USA, 2017

12. Mulder, B.; Schöberl, J.; Birke, K.P. Thermal Propagation Test Bench with Multi Pouch Cell Setup for Reproducibility Investigations. *Batteries* **2023**, *9*, 447. [CrossRef]
13. Constellium Develops New Alloys for EV Battery Enclosures. Available online: https://www.sae.org/news/2021/02/constellium-aluminum-ev-battery-enclosures (accessed on 22 September 2024).
14. *DIN 60664-1:2022*; Isolationskoordination für Elektrische Betriebsmittel in Niederspannungsanlagen—Teil 1: Grundsätze, Anforderungen und Prüfungen. VDE Verlag GmbH: Berlin, Germany, 2022.
15. Rebholz, H.; Köhler, W.; Tenbohlen, S. Dielektrische Festigkeit verschiedener Gase in GIS. In Proceedings of the Grenzflächen in elektrischen Isolierstoffen-ETG-Fachtagung, Hanau, Germany, 8–9 March 2005.
16. Sturk, D.; Rosell, L.; Blomqvist, P.; Tidblad, A.A. Analysis of Li-Ion Battery Gases Vented in an Inert Atmosphere Thermal Test Chamber. *Batteries* **2019**, *5*, 61–77. [CrossRef]
17. Birke, K.P. *Modern Battery Engineering: A Comprehensive Introduction*; World Scientific Publishing Co. Pte. Ltd.: Singapore, 2019; ISBN 9789813272156.
18. Ruiz, V.; Pfrang, A. *JRC Exploratory Research: Safer Li-Ion Batteries by Preventing Thermal propagation*; Publications Office of the European Union: Luxembourg, 2018.
19. Thomas, G. Entwicklung und Validierung eines Diagnostikverfahrens zur Analyse von Lichtbogenfluktuationen beim Gleichstromplasmaspritzen. Ph.D. Dissertation, Technische Universität Berlin, Berlin, Germany, 2019
20. Karl-Heinrich, G., Feldhusen, J., Dubbel Taschenbuch für den Maschinenbau, Springer: Berlin/Heidelberg, Germany, 2011; pp. D36–D51, ISBN 978-3-642-17305-9.
21. Geller, W. *Thermodynamik für Maschinenbauer: Grundlagen für die Praxis*, 5th ed.; Springer: Berlin/Heidelberg, Germany, 2015; ISBN 978-3-662-44960-8.

Disclaimer/Publisher's Note: The statements, opinions and data contained in all publications are solely those of the individual author(s) and contributor(s) and not of MDPI and/or the editor(s). MDPI and/or the editor(s) disclaim responsibility for any injury to people or property resulting from any ideas, methods, instructions or products referred to in the content.